Inflammation
https://doi.org/10.1007/s10753-024-02092-5

RESEARCH

Dimethyloxallyl Glycine Preconditioning Promotes the Anti-inflammatory and Anti-fibrotic Effects of Human Umbilical Cord Mesenchymal Stem Cells on Kidney Damage in Systemic Lupus Erythematosus Related to TGF-β/Smad Signaling Pathway

Anfeng Ning[1,2] · Nansong Xiao[1,2] · Xiaoqin Yu[1,2] · Hu Wang[1,2] · Chunyi Guan[1,2] · Changlong Guo[3] · Yichao Dong[3] · Xu Ma[1,2] · Hongfei Xia[1,2]

Received: 11 March 2024 / Revised: 3 June 2024 / Accepted: 27 June 2024

Abstract

Systemic lupus erythematosus (SLE) is a chronic inflammatory autoimmune disease lacking effective treatments without adverse effects. Dimethyloxallyl glycine (DMOG) enhanced mesenchymal stem cells (MSC) capabilities, but it remains unclear how DMOG-pretreatment of MSCs augments their SLE treatment. Here, we explore the therapeutic potential of DMOG-pretreated human umbilical cord MSCs (hUC-MSCs) in a mouse lupus nephritis (LN) model. In vitro experiments showed that DMOG could alleviate the mRNA levels of *tumor necrosis factor (TNF)-α*, *interferon (IFN)-γ,* and *interleukin (IL)-6* and increase the mRNA level of *IL-13* in lipopolysaccharide (LPS)-induced inflammation in hUC-MSCs. DMOG enhanced the migratory and invasive abilities of the hUC-MSCs. In vivo animal studies revealed that DMOG-pretreated hUC-MSCs exhibited more pronounced inhibition of lymphadenectasis and reduced kidney weight and urinary protein content than MSCs alone. DMOG-pretreated hUC-MSCs improved renal morphological structure and alleviated inflammatory cell infiltration and renal fibrosis, evidenced by the reduced mRNA levels of fibrosis markers, including *fibronectin (Fn)*, *collagen alpha-1 chain (Colα1)*, *collagen alpha-3 chain (Colα3)*, and *TNF-α, IFN-γ, and IL-6* cytokines. Further investigation revealed that DMOG-pretreated hUC-MSCs down-regulated the expressions of transforming growth factor (Tgf)-β1 and its downstream effectors Smad2 and Smad3, recognized as central mediators in renal fibrosis ($P < 0.05$). The findings suggest that DMOG-pretreated hUC-MSCs can augment the therapeutic efficacy of hUC-MSCs in LN by enhancing their anti-inflammatory and antifibrotic effects, and the TGF-β/Smad signaling pathway may be involved in this process.

✉ Xu Ma
genetic88@126.com

✉ Hongfei Xia
hongfeixia@126.com

[1] Reproductive and Genetic Center & NHC Key Laboratory of Reproductive Health Engineering Technology Research, National Research Institute for Family Planning (NRIFP), Beijing 100081, China

[2] Graduate Schools, Peking Union Medical College & Chinese Academy of Medical Sciences, Beijing 100730, China

[3] National Human Genetic Resources Center, National Research Institute for Family Planning (NRIFP), Beijing 100081, China

Published online: 24 July 2024

Graphical Abstract

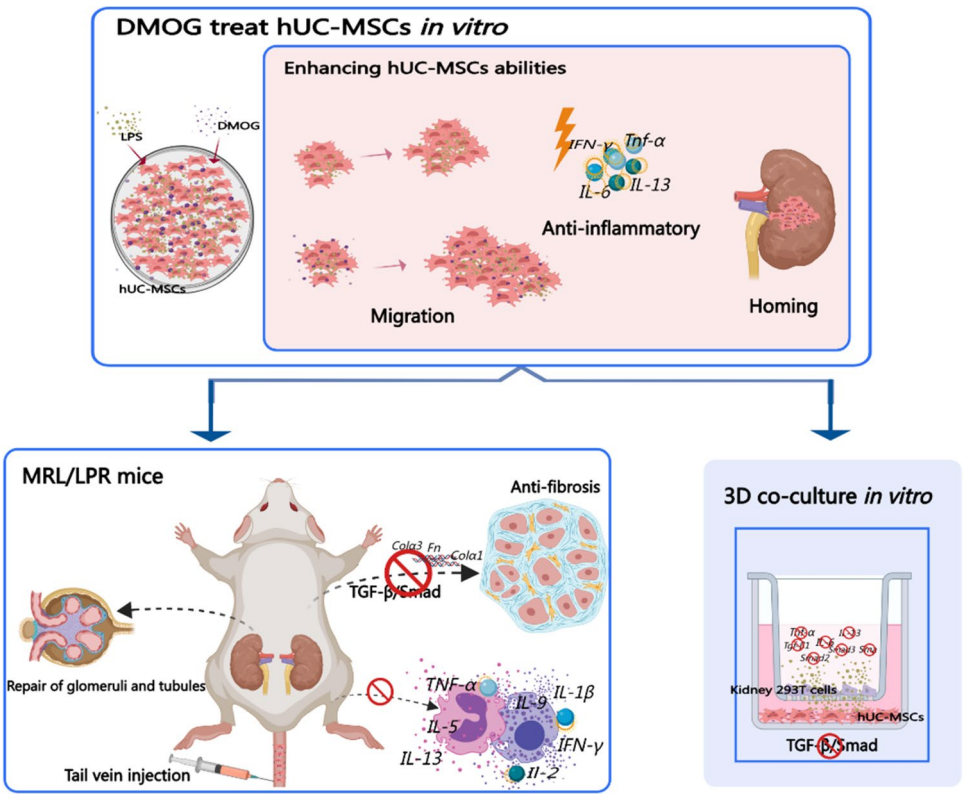

KEY WORDS human umbilical cord mesenchymal stem cells · dimethyloxallyl glycine · systemic lupus erythematosus · lupus nephritis

Introduction

Systemic lupus erythematosus (SLE) is a complex disease with an incompletely understood pathogenesis. Genetics, environmental factors, and hormones are fundamental in its development. SLE is a chronic autoimmune disease characterized by an abnormal immune system that affects healthy tissues and organs within the body [1]. Lupus nephritis (LN) is the most severe organ involvement in SLE, occurring in approximately 40–50% of SLE cases [2, 3], with an eight-fold higher mortality rate than expected [4]. Nephritis is a condition in which the disease affects the renal glomeruli, causing renal dysfunction, manifesting as glomerular inflammation, glomerular damage, reduced glomerular filtration, proteinuria, and other related phenomena [5]. High-dose corticosteroids, such as prednisone, can modulate renal inflammation; however, long-term randomized treatment trials have revealed a significantly increased risk of kidney function deterioration [6]. There is a lack of effective and low-side-effect treatments for kidney damage in SLE patients.

Stem cell therapy is an emerging treatment modality that has been investigated for various diseases, including SLE [7, 8]. However, mesenchymal stem cells (MSC) exhibit restricted homing capabilities at sites of tissue injury [9]. Shaughnessy et al. reported that a low MSCs engraftment rate of MSCs led to treatment failure in patients with SLE who underwent stem cell transplantation [10]. Transplantation of human umbilical cord MSCs (hUC-MSCs) has been shown to alleviate LN; however, the reparative outcomes are not entirely satisfactory [11]. Renal inflammation and fibrosis are hallmarks of chronic progressive kidney disease [12]. Chronic inflammatory reactions induced by various stimuli, including tissue injury, can lead to tissue fibrosis [13, 14]. In most reported experiments, the transforming growth factor (TGF)-β/Smad signaling pathway is the principal route leading to renal fibrosis. Specifically, TGF-β1 induces phosphorylation of Smad2 and Smad3, two receptor-associated smads (R-Smads), thereby promoting renal fibrosis [15]. Improving their ability to engraft damaged tissues, increasing their anti-inflammatory potential to counter SLE-related chronic inflammation, and bolstering their antifibrotic

capabilities to relieve or reverse tissue fibrosis are pivotal for optimizing SLE therapy outcomes.

Dimethyloxallyl glycine (DMOG) is a class of compounds that can activate the HIF-1α signaling pathway under normoxic conditions; these compounds are known as "hypoxia mimetic compounds," enhancing cell survival under low-oxygen conditions and promoting the migration of mesenchymal MSCs [16]. DMOG may also exert significant anti-inflammatory and immune-regulation effects, as it has been shown to modulate macrophage polarization and inhibit alveolar bone resorption in a murine periodontitis model [17].

Understanding and addressing the limitations of treating kidney damage in SLE are paramount for improving patient outcomes. MSCs therapy has immense potential and offers a promising avenue for intervention. Specifically, DMOG-pretreated hUC-MSCs have emerged as a novel approach for alleviating renal inflammation and fibrosis associated with LN. This study explored the therapeutic efficacy and underlying mechanisms of DMOG-pretreated hUC-MSCs in mitigating kidney damage associated with SLE using an MRL/lpr lupus mouse model. Elucidating the therapeutic potential of this innovative approach will contribute to developing effective treatments for SLE-associated kidney damage, thereby enhancing patient care and outcomes.

Materials and Methods

Detection of the Surface Markers and Differentiation Potential of hUC-MSCs

hUC-MSCs were purchased from Nuwacell Biotechnology Co., Ltd. (Anhui, China) and cultured in α-MEM (Gibco, USA) and 10% fetal bovine serum (FBS; Gibco, USA) at 37 °C in 5% CO_2. The morphology of the hUC-MSCs was observed using Giemsa staining. Fifth-generation hUC-MSCs were used to detect surface markers using a Human MSCs Analysis Kit (BD Biosciences, USA) and flow cytometry. Following the manufacturer's instructions, hUC-MSCs were stained with fluorochrome conjugated antibodies (PerCP, PE, APC, or FITC) serving as positive controls, and hUC-MSCs without any treatment were used as negative controls to exclude cell debris and false-positive results. From each hUC-MSCs sample, 10,000 events were acquired. hUC-MSCs stained positive for CD90, CD44, CD105, and CD73 and negative for CD34, CD11b, CD19, CD45, and HLA-DR surface molecules.

The adipogenic capacity was assessed using inducers (2 mmol dexamethasone, 2 mg/L insulin, 0.5 mmol 3-isobutyl-1-methylxanthine, 0.2 mmol indomethacin) for 14 days and assessed by Oil Red O staining to observe intracellular lipid accumulation. Osteogenic capacity was evaluated by inducers (2 mmol dexamethasone, 1 M sodium glycerol phosphate, and 10 mmol vitamin C) for 14 days and by Alizarin Red staining to evaluate calcium deposition.

Lipopolysaccharide (LPS) or DMOG Treatment of hUC-MSCs

The fifth-generation hUC-MSCs were treated with 0, 1, 5, or 10 μg/mL LPS to determine the concentrations that inhibited cell proliferation. LPS (10 μg/mL) was considered to have the most pronounced damaging effect. The previous research in our laboratory indicated that 25 μmol/L DMOG promoted the expression of HIF-1α. The experiment was divided into four groups in which hUC-MSCs were 1) not subjected to any treatment (control group), 2) treated with LPS for 24 h (LPS group), 3) treated by DMOG for 24 h (DMOG group), and 4) treated with both 10 μg/mL LPS and 25 μmol/L DMOG for 24 h (LPS + DMOG group).

Mouse Model of LN

MRL/lpr mice spontaneously generate lupus-like symptoms comparable to humans at approximately 16 weeks. To ensure that all mice had contracted the disease, 13-week-old female MRL/lpr mice (Aniphe Biolaboratory Inc., Jiangsu, China) were selected for the study; samples were taken at 18 weeks. Age-matched C57BL/6 J mice (Beijing HFK Bioscience Co. Ltd., Beijing, China) served as controls. The mice were housed in a specific pathogen-free facility under controlled indoor conditions, including a 60-decibel noise level, a temperature of 25 °C, and a 7 AM to 5 PM light cycle. They were provided sterile feed and clean drinking water. All animal procedures adhered to the ethical standards and were approved by the Institutional Animal Care and Laboratory Animal Welfare Ethics Committee of the National Research Institute for Family Planning.

Treatment and Grouping in a Mouse Model of LN

Forty 13-week-old female MRL/lpr mice and ten age-matched C57BL/6 J mice were randomly selected for this study. The treatment involved transplanting 10^6 hUC-MSCs/200 μL saline solution via tail vein injection once weekly for five treatments. Tissues were sampled seven days after the fifth injection of hUC-MSCs. The experiment comprised five distinct groups: the control group utilized normal C57BL/6 J mice as a reference, the model group employed MRL/lpr mice to simulate the state of LN, the sham group consisted of MRL/lpr mice receiving saline treatment as a sham control, the MSC group involved MRL/lpr mice receiving untreated hUC-MSCs, and the DM group consisted of MRL/lpr mice receiving hUC-MSCs pretreated with 25 μmol/L DMOG for 24 h.

Quantitative Real-Time Polymerase Chain Reaction (qRT-PCR)

qRT-PCR was used to detect the mRNA expression levels of selected genes. Total RNA was extracted using the TRIzol reagent (Invitrogen, USA). Total RNA (1 μg) was reverse transcribed into cDNA using a reverse transcription kit (Trans Gen Biotech, Beijing, China). qPCR was performed using SYBR Green (Bio-Rad, Hercules, CA, USA) and the primers shown in Table 1.

Cell Counting kit-8 (CCK-8)

The CCK-8 assay was used to detect cell proliferation. LPS-treated cells were incubated at different concentrations for 12, 24, 48, or 72 h. After each incubation period, CCK-8 was added to the cell culture and incubated for 30 min. Cell viability was measured using a microplate reader (Biotek Biological Technology Co., Ltd., Shanghai, China) at a wavelength of 450 nm.

Cell Scratch Assay

A cell scratch assay was used to assess the cell migration and repair capacity. After hUC-MSCs fifth generations had grown to approximately 90%, a 20 μL pipette tip was used to create wounds. Following this controlled injury, a structured time-lapse observation protocol was initiated, with the wound sites examined, documented, and captured at 0, 6, 12, 18, and 24 h after the initial injury.

In Vitro Cell Migration Assay

Transwell inserts (24 mm) with 8 μm pores membrane chamber (Corning Costar Corp., USA) were used to detect the cell migration. hUC-MSCs (10^6 cells/mL) alone or treated with 25 μmol/L DMOG or 10 μg/mL LPS were seeded in the top of an 8.0 μm pore membrane chamber and cultured with 1% FBS. A cell culture medium containing 10% FBS was placed in the lower chamber to establish a concentration gradient to induce cell migration. After 24 h of incubation, cells that adhered to the bottom of the membrane were fixed with 4% paraformaldehyde for 30 min, stained with crystal violet for 15 min, imaged, and counted.

Immunofluorescence (IF)

Immunofluorescence was used to detect anti-human nuclei to determine whether the hUC-MSCs had migrated to the kidneys. Kidney slides were incubated with mouse anti-human nuclei monoclonal antibody (Abcam, Cambridge, MA, USA) at 4 °C overnight. The primary antibody was replaced with 10% goat serum as a negative control. The slices were

Table 1 Primer Sequences

Gene name	Primer sequence
H-*C/EBP-α*-F	CCGCCTTCAACGACGAGTTC
H-*C/EBP-α*-R	TAGTCAAAGTCGCCGCC
H-*GAPDH*-F	CAAGAGCACAAGAGGAAGAGAG
H-*GAPDH*-R	CTACATGGCAACTGTGAGGAG
H-*IFN-γ*-F	CCCATGGGTTGTGTGTTTATTT
H-*IFN-γ*-R	AAACCGGCAGTAACTGGATAG
H-*IL-13*-F	GCTCTCAGCCAACGAGTAAT
H-*IL-13*-R	CAGTGTTCAAGGTACCCTTCTAT
H-*IL-6*-F	CCAGGAGAAGATTCCAAAGATGTA
H-*IL-6*-R	CGTCGAGGATGTACCGAATTT
H-*OPN*-F	CCGAGGTGATAGTGTGGTTTATG
H-*OPN*-R	CTTTCCATGTGTGAGGTGATGT
H-*PPAR-γ*-F	TTCCATTCACAAGAACAGATCC
H-*PPAR-γ*-R	CTTTGATTGCACTTTGGTACTC
H-*RUNX2*-F	GGTACCAGATGGGACTGTG
H-*RUNX2*-R	CATAACAGCAGAGGCATTCC
H-*SMAD2*-F	CTGATCTTATCTCCGGGCTCTA
H-*SMAD2*-R	GGGAGGAGGTTGAGAATGAAAG
H-*SMAD3*-F	ACAGGAGATGTAGGGAGAAGAA
H-*SMAD3*-R	CTCTAGCCAAGTCACACAGTAAG
H-*SMA*-F	CTGTGAGAAGGGTGTTGTAGTT
H-*SMA*-R	CCACATACGCCTCACATACAT
H-*TGF-β1*-F	TTCAGTCACCATAGCAACACTC
H-*TGF-β1*-R	GAACTCCTCCCTTAACCTCTCT
H-*TNF-α*-F	GATCCCTGACATCTGGAATCTG
H-*TNF-α*-R	GAAACATCTGGAGAGAGGAAGG
M-*Cola1*-F	AGGTGCTATTTAACAAGGGAGAA
M-*Cola1*-R	AGATAGGCCCAGGAACTAGAA
M-*Cola3*-F	GGCCTCCCAGAACATTACATAC
M-*Cola3*-R	TTTGATCCCATCAGCTTCAGAG
M-*Fn*-F	GTGCTTCATGCCGCTAGAT
M-*Fn*-R	GTGTGGATTGACCTTGGTAGAG
M-*Gapdh*-F	CAAGGACACTGAGCAAGAGAG
M-*Gapdh*-R	GGGTCTGGGATGGAAATTGT
M-*Ifn-γ*-F	CTCTTCCTCATGGCTGTTTCT
M-*Ifn-γ*-R	TTCTTCCACATCTATGCCACTT
M-*Il-13*-F	GCTCTTGCTTGCCTTGGTG
M-*Il-13*-R	GGGAGTCTGGTCTTGTGTGATG
M-*Il-1β*-F	AAAAAGCCTCGTGCTGTCGG
M-*Il-1β*-R	GTGGGTGTGCCGTCTTTCAT
M-*Il-2*-F	ATGATGAGTCAGCAACTGTGGTG
M-*Il-2*-R	CATAGTTATTGAGGGCTTGTTGAGA
M-*Il-5*-F	TGCATCAGGGTCTCAAGTATTC
M-*Il-5*-R	GGATGCTAAGGTTGGGTATGT
M-*Il-9*-F	GGGCATCAGAGACACCAATTA
M-*Il-9*-R	ATCAGTTGGGACGGAGAGA
M-*Smad2*-F	AGCTGGTATGCTGGTGTTC
M-*Smad2*-R	CTCAGTGCTGGGTGTAGTTTAG
M-*Smad3*-F	GTTTAGCATTCTGCCGCTTTC
M-*Smad3*-R	TCCTCAGGAGAGAGACCTTTAC

Table 1 (continued)

Gene name	Primer sequence
M-*Sma*-F	CATATTAGGGCTGGAGAATTGGA
M-*Sma*-R	CCATGAGGGTACTAGGAGTAGAG
M-*Tgf-β1*-F	GGTGGTATACTGAGACACCTTG
M-*Tgf-β1*-R	CCCAAGGAAAGGTAGGTGATAG
M-*Tnf-a*-F	TTGCTCTGTGAAGGGAATGG
M-*Tnf-a*-R	GGCTCTGAGGAGTAGACAATAAAG

then incubated with the secondary antibody labeled with fluorescein isothiocyanate-conjugated (FITC) conjugated goat anti-mouse IgG (Abcam, Cambridge, MA, USA) for one hour at 37 °C. Nuclei were counterstained with DPAI (Abcam, Cambridge, MA, USA) and the slides were sealed. The sections were viewed under an inverted fluorescence microscope (Leica Microsystems, Wetzlar, Germany).

Hematoxylin–eosin (HE) Staining

The tissues were stained to observe the morphological structure of the kidneys. Slices (4 μm) were stained with hematoxylin for two minutes, followed by eosin for one minute. The slides were washed, dehydrated, cleaned, and mounted on glass slides for microscopic examination (Leica Microsystems CMS GmbH).

Measurement of Urine Protein Concentration

Urine samples were collected from the animals before each treatment session was performed to measure urinary protein levels. Bovine serum albumin (BSA) (dilution concentrations of standards: 1 mg/mL, 0.8 mg/mL, 0.6 mg/mL, 0.4 mg/mL, and 0.2 mg/mL) and the urine samples were mixed with Coomassie brilliant blue staining solution for 10 min. Absorbance was measured at 595 nm using a microplate reader (Biotek Biological Technology Co., Ltd., Shanghai, China). The urinary protein concentration was calculated based on a standard curve and absorbance values of the urine samples.

Enzyme-linked Immunosorbent Assay (ELISA)

ELISA was used to detect the protein levels of antinuclear antibody (ANA), small nuclear ribonucleoprotein (snRNPSm), and anti-double-stranded DNA (dsDNA) antibody in the serum samples, following the manufacturer's instructions (Jiangsu Meian Industrial Co., LTD., China). Purified antibodies were coated onto microplates to create solid-phase antibodies. Antigens were added sequentially to the wells coated with monoclonal antibodies. They were then combined with antibodies labeled with horseradish peroxidase (HRP) to form an antibody-antigen-enzyme complex. After thorough washing, tetramethylbenzidine (TMB) was added to the substrate for color development at 37° C for 10 min in the dark. TMB was converted to blue in the presence of horseradish peroxidase (HRP) and yellow under acidic conditions. The intensity of the color was positively correlated with the amount of the target protein in the samples. The absorbance values (OD values) were measured at a wavelength of 450 nm using a microplate reader (Tecan Shanghai Experimental Equipment Co., Ltd., China). The protein concentration in the mouse serum samples was calculated using a standard curve.

Periodic Acid-Schiff (PAS) Staining

A glycogen PAS staining kit (Nanjing Senbejia Biotechnology Co., Ltd., Nanjing, China) was used to detect the structure of the renal tubules and glomeruli. Paraffin-embedded kidney tissue sections were subjected to standard deparaffinization and hydration, then immersed in a periodic acid solution for five minutes at room temperature, followed by staining with Schiff's reagent for 15 min in the dark. Subsequently, the sections were stained with hematoxylin for one minute to highlight the cell nuclei. An acidic alcohol differentiation solution was briefly applied to adjust the staining intensity.

Masson's Trichrome

A Masson's trichrome staining kit (Solebao Technology Co., Ltd., Beijing, China) was used to measure renal fibrosis. The hydrated paraffin sections were stained with hematoxylin for five minutes, differentiated in acidic alcohol for 10 s, and immersed in Masson's blue solution for five minutes for blue staining. Subsequently, the sections were stained with Ponceau red for five minutes and then with aniline blue for one minute. Rapid dehydration was achieved using 95% ethanol for three seconds and with absolute ethanol twice for 5–10 s each time. The sections were cleared with xylene twice for 1–2 min and mounted with a neutral resin for preservation.

Immunohistochemistry (IHC)

IHC was used to examine the protein expression and localization. After dewaxing and hydrating kidney tissue paraffin sections, antigens were retrieved using pepsin (Beijing Zhong Shan Golden Bridge Biological Technology Co., Ltd., China) at 37 °C for 10 min. Endogenous peroxidase was blocked using 3% H_2O_2, followed by incubation with goat serum at room temperature for one hour to block non-specific binding sites. Rabbit and mouse monoclonal antibodies (Tgf-β1, Sigma-Aldrich (St. Louis, MO, USA), Smad2/3 (Sigma-Aldrich, St. Louis., MO, USA), p-Smad2

(Sigma-Aldrich, St. Louis., MO, USA), and p-Smad3 (Suzhou Bo'aolong Technology Co., Ltd.) were then added and allowed to incubate overnight at 4 °C, followed by incubation with an HRP-conjugated goat anti-rabbit or anti-mouse IgG (Abcam, Cambridge, MA, USA) at 37 °C for one hour. Sections were stained with diaminobenzidine using a DAB chromogenic staining kit (Beijing Zhong Shan Golden Bridge Biological Technology Co., Ltd., China), followed by counterstaining nuclei with hematoxylin. Samples were observed and imaged using an inverted fluorescence microscope (Leica Microsystems CMS GmbH, Germany). The images were analyzed semi-quantitatively using ImageJ software (National Institutes of Health, USA).

Western Blot (WB)

The protein expression levels of the selected genes were quantified using western blotting The protein lysates were boiled and loaded onto a 12% polyacrylamide gel. After electrophoresis, the proteins were transferred onto a PVDF membrane. The membrane was incubated overnight at 4 °C with antibodies against Tgf-β1 (Sigma-Aldrich, St. Louis., MO, USA.), Smad2/3 (Sigma-Aldrich, St. Louis., MO, USA.) p-Smad2 (Sigma-Aldrich, St. Louis., MO, USA.), p-Smad3 (Suzhou Bo'aolong Technology Co., Ltd., China.), and Sma (Suzhou Bo'aolong Technology Co., Ltd., China). Specific protein-antibody complexes were detected using HRP-conjugated secondary antibodies and quantified by chemiluminescence.

The Membrane-based 3D Co-culturing System

To analyze the effect of hUC-MSCs alone or treated with DMOG on renal cells with inflammatory injury, 24 mm Transwell inserts and plates with 0.4 μm pores (Corning Inc., USA) were used to establish the membrane-based 3D co-culturing system. The pore size of 0.4 μm allowed the molecular exchange between the upper and lower chambers. Human embryonic kidney 293 T cells (HEK 293 T cells) alone or treated by 10 μg/mL LPS obtained from the former in vitro cell experiment were seeded at the bottom of the upper chamber, and hUC-MSCs alone or treated by 25 μmol/L DMOG obtained by a preliminary experiment were seeded at the lower chamber and co-cultured for 48 h. HEK 293 T cells in the upper chambers were collected for downstream analyses, including crystal violet staining and qRT-PCR.

Crystal Violet Staining

The upper chamber 293 T cells were stained by crystal violet as follows: ethanol (100%; 100 μL) was added to each well and fixed for 15 min. After being washed twice with PBS, 100 μL of 4% crystal violet dye was added to each well and kept at room temperature for 15 min. The excess dye was slowly washed away with running water; the plates were air-dried on absorbent paper, and the cells were counted.

Statistical Analysis

Data were analyzed using the GraphPad Prism software (Mac version 9.0.0; GraphPad Software, San Diego, California, USA). The experimental data were divided into no less than three groups, and the results were expressed as mean ± standard deviation. Independent sample *t*-tests were used to compare the means between two groups, whereas one-way analysis of variance (ANOVA) was used for comparisons involving multiple groups. Data were considered significantly different when $P < 0.05$ (denoted as * for $P < 0.05$ and ** for $P < 0.01$, $n \geq 3$).

Results

Detection of hUC-MSCs Surface Antigen and Differentiation Potential

The study characterized and analyzed hUC-MSCs to gain insights into their properties.

The study was initiated by examining the morphological features of hUC-MSCs after two days under standard culture conditions. Microscopic observations revealed that the cells were plastically adherent and had a spindle-shaped morphology, a hallmark of mesenchymal hUC-MSCs, indicating standard growth (Fig. 1A). Giemsa staining revealed uniform distribution of cell nuclei and cytoplasm (Fig. 1B).

To establish the hUC-MSCs' identity, flow cytometry assessed the expression of specific surface markers, showing that CD90, CD44, CD105, and CD73 surface markers on hUC-MSCs were present at > 97%. Conversely, CD34, CD11b, CD19, CD45, and HLA-DR surface markers appeared at < 1% (Fig. 1C).

Based on the surface marker analysis, we explored the functional capabilities of hUC-MSCs. In particular, we investigated the potential of adipogenic and osteogenic differentiation. After 14 days of induction, the cells formed characteristic lipid droplets (Fig. 1D) and calcium nodules (Figs. 1E and F), indicating their capacity to differentiate into adipose and bone tissues.

mRNA expression analysis revealed a significant upregulation of adipogenesis (*C/EBP-α* and *PPAR-γ*) and osteogenesis (*RUNX2* and *OPN*) in the MSC and DM groups compared with the control group ($P < 0.01$) (Figs. 1 G and H), providing further evidence of their multipotent differentiation capacity.

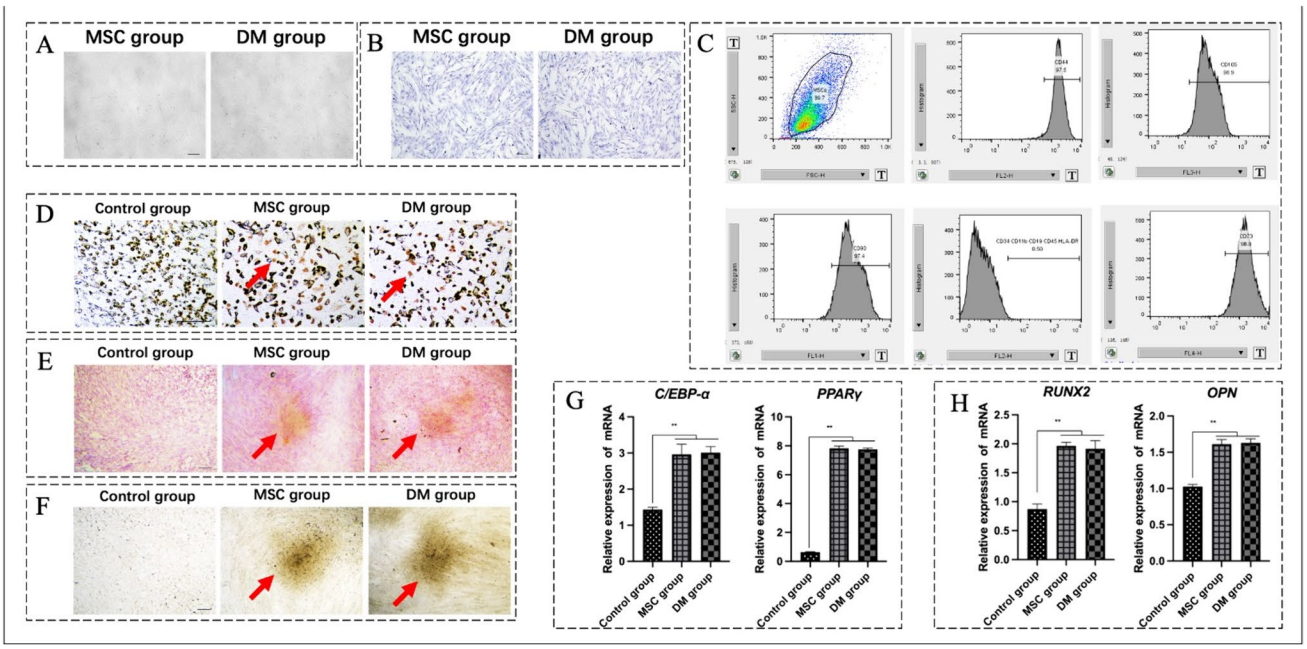

Fig. 1 Characterization of biological properties of hUC-MSCs. (**A**) Observation of hUC-MSCs morphology. (**B**) Observation of Giemsa-stained hUC-MSCs morphology. The cytoplasm stained blue, and the cell nuclei stained blue-purple. (**C**) Flow cytometry identified hUC-MSCs surface markers; 10,000 events were acquired from the hUC-MSCs sample. CD44 with PE, CD105 with PerCP, CD90 with FITC, CD34, CD11b, CD19, CD45 and HLA-DR with PE, CD73 with APC. (**D**) Detection of induced hUC-MSCs adipose differentiation results by Oil Red O staining. The lipid droplets were stained red (red arrow). (**E**) Detection of induced hUC-MSCs calcium nodule differentiation results by alizarin red staining. The calcium nodules were stained orange-yellow (red arrow). (**F**) Detection of induced hUC-MSCs calcium nodule differentiation results by ALP staining. The calcium nodules were stained black (red arrow). (**G**) Detection of the expression of lipogenic marker genes (*C/EBP-α* and *PPARγ*) by qRT-PCR. (**H**) Detection of the expression of osteogenic marker genes (*RUNX2* and *OPN)* by qRT-PCR. Scale bar: 100 μm. Control group: hUC-MSCs uninduced. MSC group: hUC-MSCs by adipogenic or osteogenic induction. DM group: hUC-MSCs treated with 25 μmol/L DMOG by adipogenic or osteogenic induction. The data were analyzed by one-way ANOVA and expressed as mean ± standard deviation (SD) (n = 3; **: $P < 0.01$).

DMOG Increases the Anti-Inflammatory and Homing Properties of hUC-MSCs

Having established the fundamental characteristics of hUC-MSCs, we explored how the cells respond to an inflammatory environment and whether DMOG influences the migration and invasion behaviors associated with homing [18].

Lipopolysaccharide (LPS) was used as a trigger to induce inflammation-related damage in hUC-MSCs. Our preliminary CCK-8 experiments identified the optimal injury conditions as a 24-h exposure to 10 μg/mL LPS leading to the most significant damage effect compared to the 0 μg/mL LPS group ($P < 0.05$) (Fig. 2A); we investigated the effect of DMOG on hUC-MSCs.

We first assessed the changes in cytokine mRNA levels in hUC-MSCs following inflammatory stimulation using qRT-PCR. When compared to the LPS group, the LPS + DMOG group showed significant downregulation of *tumor necrosis factor (TNF)-α* ($P < 0.05$), *interferon (IFN)-γ* ($P < 0.01$), and *interleukin (IL)-6* ($P < 0.05$), along with significant upregulation of *IL-13* ($P < 0.05$) (Fig. 2B).

Inflammation is closely associated with the migratory capacity of hUC-MSCs [19]. We investigated whether DMOG treatment affected hUC-MSCs migration and invasion. Scratch assays indicated that, compared to the LPS group, DMOG treatment significantly improved cell migration at the wound site, particularly after 24 h of treatment in the LPS + DMOG group ($P < 0.05$) (Fig. 2C). The invasion assay showed that the number of cells in the LPS + DMOG group was significantly higher than in the LPS group ($P < 0.05$) (Fig. 2D).

Based on these results, we speculated that DMOG treatment may enhance the homing ability of hUC-MSCs. We used human-specific nuclear antibodies to bind animal kidney samples to validate this hypothesis. Remarkably, there was no signal expression in the model and sham groups. In contrast, the DM group exhibited higher signal expression than the MSC group, suggesting the presence of stem cell engraftment in both the MSC and DM groups, with potentially greater homing efficiency in the DM group (Fig. 2E).

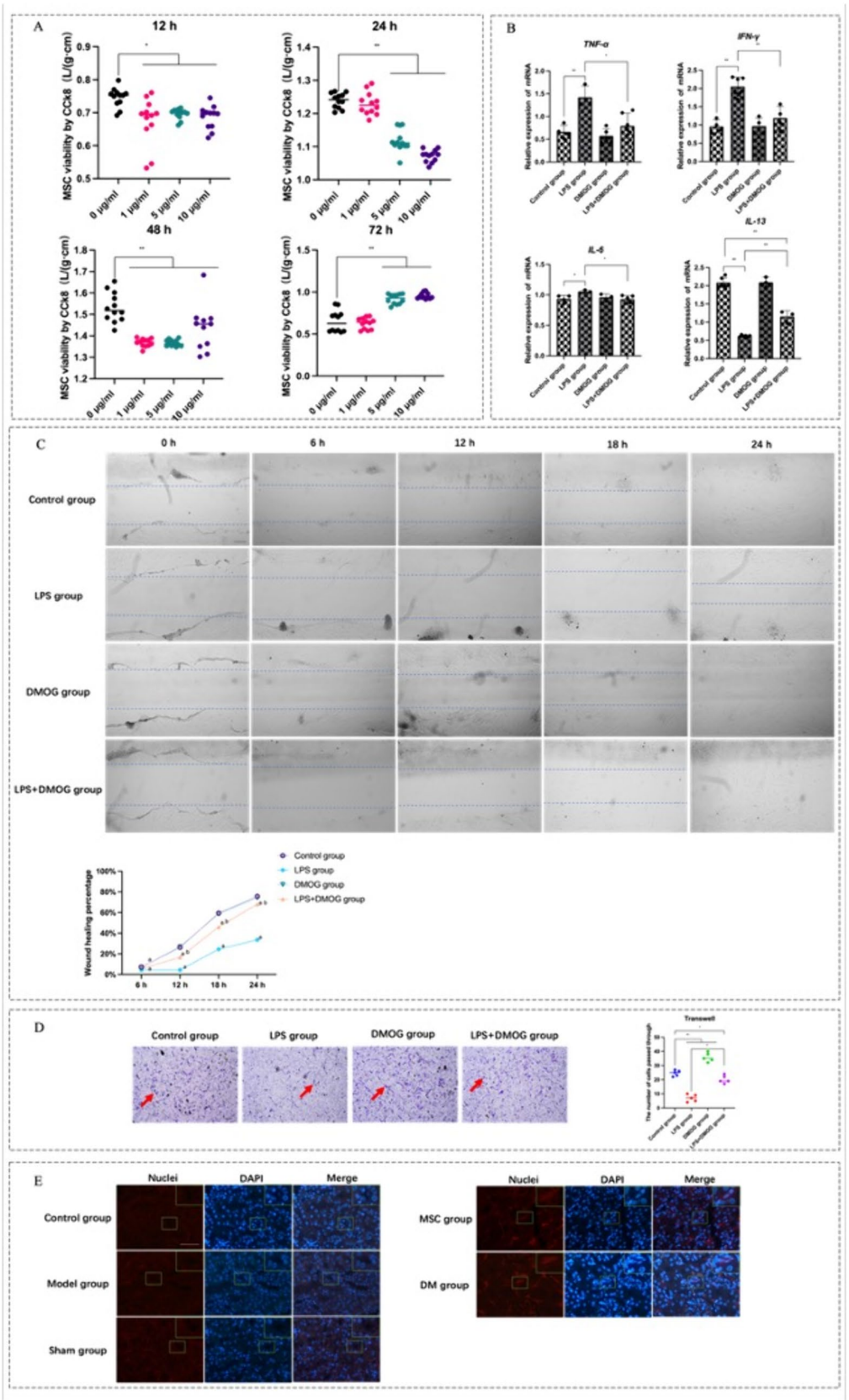
A
12 h
24 h
48 h
72 h
MSC viability by CCk8 (L/(g·cm))
0 μg/ml
1 μg/ml
5 μg/ml
10 μg/ml
B
TNF-α
IFN-γ
IL-6
IL-13
Relative expression of mRNA
Control group
LPS group
DMOG group
LPS+DMOG group
C
0 h
6 h
12 h
18 h
24 h
Control group
LPS group
DMOG group
LPS+DMOG group
Wound healing percentage
D
Control group
LPS group
DMOG group
LPS+DMOG group
Transwell
E
Nuclei
DAPI
Merge
Control group
Model group
Sham group
MSC group
DM group

◂**Fig. 2** Assessing the in vitro effects of DMOG on anti-inflammatory properties, migration, invasion, and homing in repairing hUC-MSCs within an LPS-induced injury cell model. (**A**) Assessing the impact on hUC-MSCs viability following treatment with LPS at different concentrations and durations by CCK-8. (**B**) Detection of the expression of inflammatory genes (*TNF-α*, *IFN-γ*, *IL-6,* and *IL-13*) of hUC-MSCs by qRT-PCR. (**C**) hUC-MSCs migration ability determined by Scratch. The blue dashed lines indicate the boundaries of cell growth. Scale bar: 100 μm. The data were analyzed by one-way ANOVA and expressed as mean ± SD (n = 3; a: $P < 0.05$ vs. control group; b: $P < 0.05$ vs. LPS group). (**D**) hUC-MSCs invasion ability by Transwell. The passing cells were stained purple by crystal violet (red arrow). Scale bar: 100 μm. Control group: untreated hUC-MSCs. LPS group: hUC-MSCs treated with 10 μg/mL LPS. DM group: hUC-MSCs treated with 25 μmol/L DMOG. LPS + DMOG group: hUC-MSCs treated with 10 μg/mL LPS and 25 μmol/L DMOG (**E**) hUC-MSCs homed to the kidney as determined by immunofluorescence. The positive signal is indicated by red fluorescence. Scale bar: 20 μm. Control group: C57BL/6 J mice. Model group: MRL/lpr mice. Sham group: MRL/lpr mice receiving saline treatment. MSC group: MRL/lpr mice receiving untreated hUC-MSCs. DM group: MRL/lpr mice receiving hUC-MSCs treated with 25 μmol/L DMOG. The data were analyzed by one-way ANOVA and expressed as mean ± SD (n ≥ 3; *: $P < 0.05$, **: $P < 0.01$).

DMOG Preconditioning Enhances the Protective Effects of hUC-MSCs on Neck Lymph Nodes and Kidney Tissues in SLE

Our preliminary experimental results indicated that DMOG may enhance the anti-inflammatory and accumulation abilities of hUC-MSCs in damaged areas. Furthermore, the dissection and analysis of mice from various treatment groups revealed promising outcomes.

During dissection, enlargement of the lymph nodes in the neck and under the skin was seen in both the model and sham groups. MSC transplantation exhibited a trend toward reduced lymphadenectasis. In contrast, DMOG-pretreated hUC-MSCs transplantation visibly reduced the enlargement of lymph nodes, approaching the size of normal lymph nodes observed in the control group (Fig. 3A). Subsequently, tissues from the neck lymph nodes (Fig. 3B), kidneys (Fig. 3C), spleen (Fig. 3D), and thymus (Fig. 3E) of mice in each group were harvested and examined. The model and sham groups showed significant organ enlargement, whereas the MSC and DM groups showed signs of recovery, with the DM group showing the most notable improvement. Subsequent statistical analysis of organ coefficients revealed significant restoration of neck lymph nodes ($P < 0.01$) and kidney tissues ($P < 0.05$) in the DM group compared to the model group (Fig. 3F).

Alleviation of Renal Tubular Protein Cast Formation and Inflammatory Cell Infiltration by DMOG-Pretreated hUC-MSCs

We investigated the effects of renal repair from a microscopic phenotypic viewpoint. Significant formation of protein casts within the renal tubules was observed in both the model and sham groups, accompanied by pronounced infiltration of inflammatory cells into the renal interstitium. Compared with the model group, although there was a reduction in protein casts and inflammatory cell infiltration in the MSC group ($P < 0.01$), the effects were still somewhat present. Conversely, in the DM group, the formation of protein casts was almost absent, and the degree of inflammatory cell infiltration in the renal interstitium was significantly reduced ($P < 0.01$) (Figs. 4 A and B).

hUC-MSCs with/without DMOG Restore the Protein Content in the Urine and SLE-Specific Antibody Levels in the SLE Mouse Model

Expanding on the favorable outcomes observed in the renal analysis, we assessed the efficacy of DMOG treatment through two additional measures: monitoring urinary protein levels at various time points within each group and examining the hallmark SLE antibodies present in the animal sera. The results of these examinations shed further light on the potential of DMOG treatment in mitigating renal abnormalities associated with SLE.

By monitoring the urinary protein levels at different time points within each group, after the fifth treatment, the urine protein content in the DM group was found to be significantly lower than that in the model group ($P < 0.05$) (Fig. 5A). Examining the hallmark SLE antibodies, including antinuclear antibodies (ANA), small nuclear ribonucleoprotein (snRNPSm), and anti-double-stranded DNA antibodies (dsDNA), in animal sera, showed that the antibody levels in the DM group were closer to the control group ($P > 0.05$) (Fig. 5B), suggesting that DMOG-pretreated hUC-MSCs exert positive effects on the course of SLE through multiple mechanisms.

DMOG Treatment Enhances the Anti-Inflammatory and Antifibrotic Effects of hUC-MSCs on Kidney Damage in SLE

We conducted a series of experiments to validate the regenerative potential of DMOG-pretreated hUC-MSCs for renal damage repair and ensure precise and robust analytical outcomes. This multifaceted approach allowed us to thoroughly scrutinize the results and thus provide a holistic and accurate assessment.

In the PAS experiment, noteworthy histological changes were evident in the model and sham groups, with observable features including exposed cell nuclei on the glomerular basement membrane, detachment of tubular brush borders, conspicuous damage to epithelial cells, and even cellular fragmentation within the renal tubules. A significant reduction in the number of epithelial cells on the tubular basement

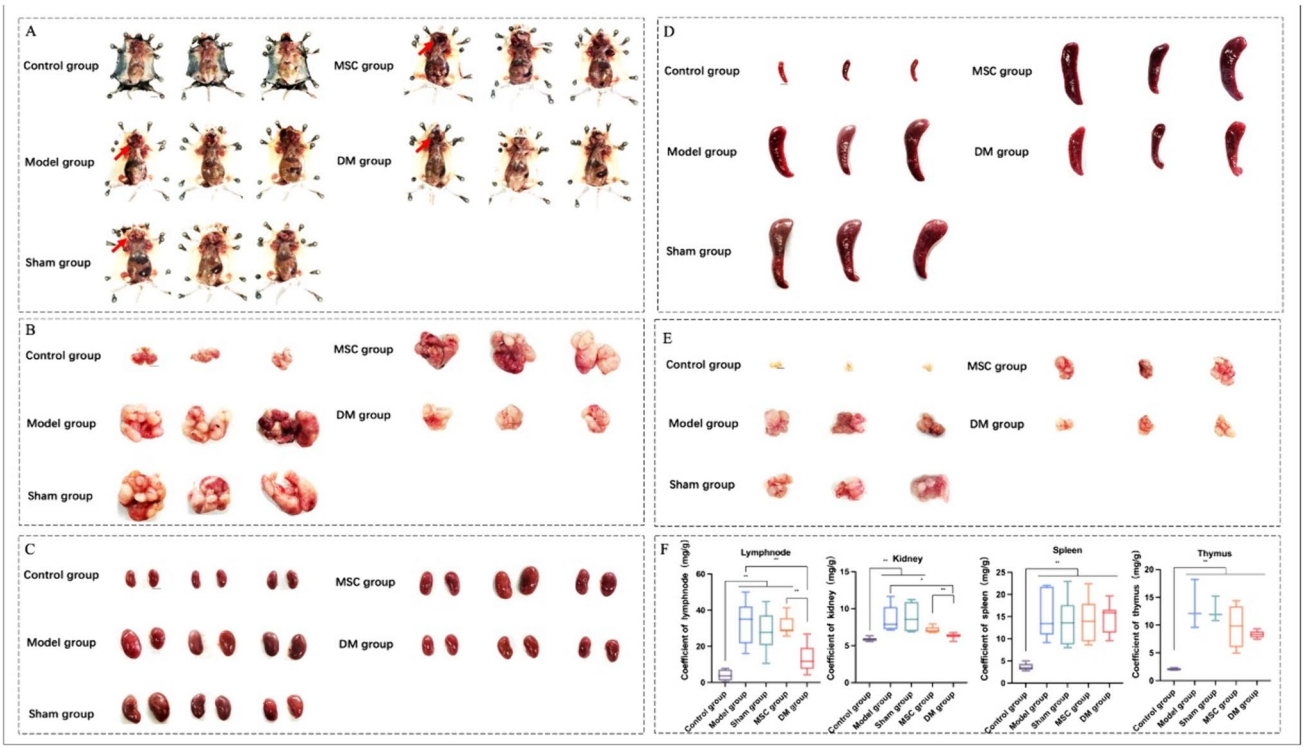

Fig. 3 Animal tissue histological examination and organ coefficient analysis. (**A**) The visual observation of mice appearance. The red arrows refer to lymph nodes. Scale bar: 1 cm. (**B**) The macroscopic appearance in cervical lymph nodes. Scale bar: 0.5 cm. (**C**) The macroscopic appearance of the kidneys. (**D**) The macroscopic appearance of the spleen. Scale bar: 0.5 cm. (**E**) The macroscopic appearance of the thymus. Scale bar: 0.5 cm. (**F**) Statistical analysis of organ coefficient. Control group: C57BL/6 J mice. Model group: MRL/lpr mice. Sham group: MRL/lpr mice receiving saline treatment. MSC group: MRL/lpr mice receiving untreated hUC-MSCs. DM group: MRL/lpr mice receiving hUC-MSCs treated with 25 μmol/L DMOG. Except for the comparison with the MSC group by *t*-test, the rest of the data were analyzed by one-way ANOVA and expressed as mean ± SD ($n \geq 3$; *: $P < 0.05$, **: $P < 0.01$).

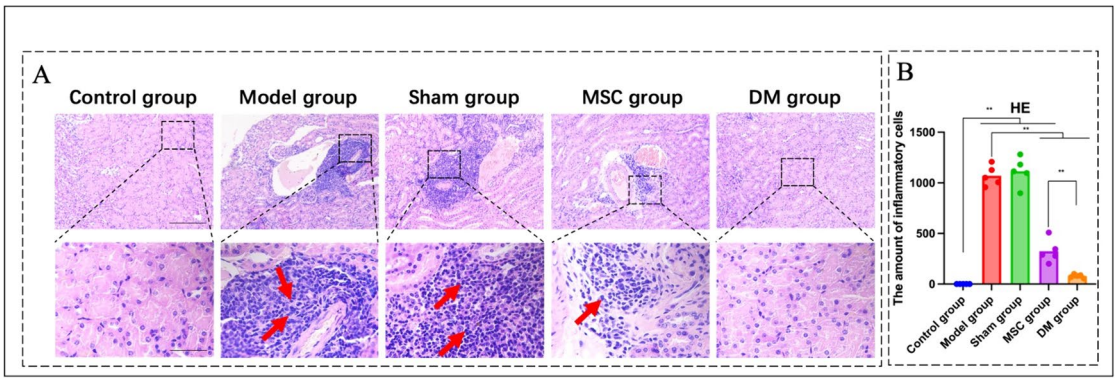

Fig. 4 Distribution of renal inflammation and protein tubule. (**A**) Examining the renal microstructure by HE. The red arrows refer to the inflammatory cells. (**B**) The number of inflammatory cells was statistically analyzed. Scale bar: 100 μm (top), 20 μm (bottom). Control group: C57BL/6 J mice. Model group: MRL/lpr mice. Sham group: MRL/lpr mice receiving saline treatment. MSC group: MRL/lpr mice receiving untreated hUC-MSCs. DM group: MRL/lpr mice receiving hUC-MSCs treated with 25 μmol/L DMOG. Except for the comparison with the MSC group by *t*-test, the rest of the data were analyzed by one-way ANOVA and expressed as mean ± SD ($n = 5$; **: $P < 0.01$).

membrane exposed it. By contrast, the MSC and DM groups exhibited varying degrees of restoration. In the DM group, the glomerular basement membrane gradually regained nuclear coverage, tubular brush borders were restored, epithelial cell damage within the renal tubules was less pronounced, and the number of epithelial cells in the tubular

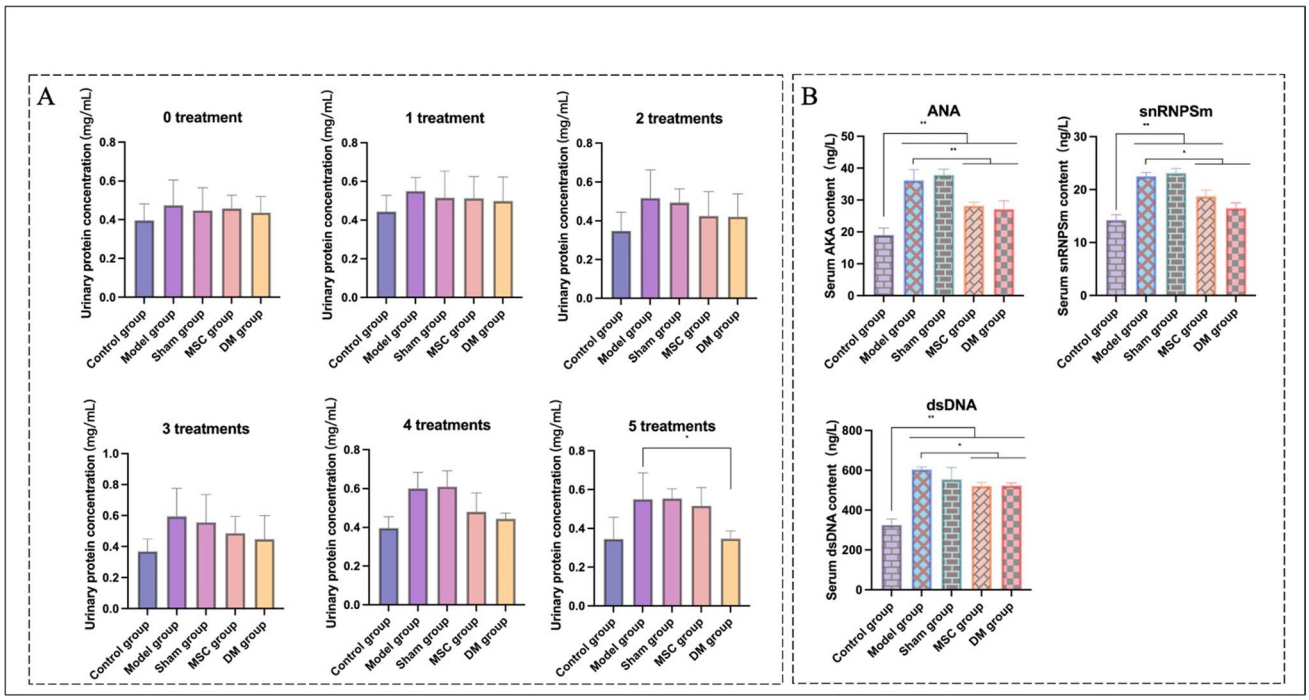

Fig. 5 Quantifying protein content in urine and assessing SLE-specific antibody levels. (**A**) Urinary protein levels at different treatment times by Bradford. (**B**) SLE hallmark antibodies (ANA, snRNPSm, and dsDNA) levels in serum by Elisa. Control group: C57BL/6 J mice. Model group: MRL/lpr mice. Sham group: MRL/lpr mice receiving saline treatment. MSC group: MRL/lpr mice receiving untreated hUC-MSCs. DM group: MRL/lpr mice receiving hUC-MSCs treated with 25 μmol/L DMOG. The data were analyzed by one-way ANOVA and expressed as mean ± SD (n = 3; *: $P < 0.05$, **: $P < 0.01$).

basement membrane progressively increased, culminating in the formation of a more intact basement membrane (Fig. 6A).

Masson's trichrome staining showed that the model and sham groups displayed noticeable thickening of the renal tubular basement membrane and similar thickening of the glomerular and renal capsule basement membranes. The proliferation of mesangial cells within the glomerular mesangium and nodular sclerosing lesions (blue nodules) were evident, collectively presenting a lobulated architecture. A significant increase in red blood cells was seen in the renal interstitium. The DM group exhibited marked reparative effects compared to the MSC group. The renal tubular basement membrane gradually returned to its normal thickness, reversing the thickening of the glomerular and renal capsule basement membranes. Reduced mesangial cell proliferation and amelioration of nodular sclerosing lesions were observed in the glomeruli, leading to a more normal structural appearance. When assessing the level of fibrosis statistically, the DM group exhibited a more significant degree of recovery compared to the MSC group ($P < 0.05$) (Fig. 6B).

In the subsequent analysis, we used qRT-PCR to detect the mRNA levels of cytokines in the renal tissues; compared with the model group, *Tnf-α* ($P < 0.01$), *Il-1β* ($P < 0.01$), *Ifn-γ* ($P < 0.05$), *Il-2* ($P < 0.01$), *Il-9* ($P < 0.01$), and *Il-5* ($P < 0.05$) were significantly down-regulated and *Il-13* ($P < 0.05$) was significantly up-regulated in the DM group (Fig. 6C). The mRNA expressions of *fibronectin (Fn)* ($P < 0.05$), *collagen alpha-1 chain (Colα1)* ($P < 0.05$), *collagen alpha-3 chain (Colα3)* ($P < 0.01$), and fibrosis-related genes were also significantly decreased in DM group compared to MSC group (Fig. 6D).

TGF-β/Smad Signaling Pathway Activation is Inhibited by DMOG-Pretreated hUC-MSCs in Renal Fibrosis of the SLE Mouse Model in Vivo and in Vitro

In a preliminary study, we discovered that SLE may lead to renal tissue fibrosis, a crucial pathological feature of the disease. The primary objective of this study was to investigate whether the renal tissues of the SLE model exhibited activation of the classical TGF-β/Smad signaling pathway, a key mechanism in the fibrotic process.

Through in-depth molecular biology and immunohistochemical analyses, we examined the relevant factors of the TGF-β/Smad signaling pathway in renal tissues. The results showed that compared with the control group, the mRNA levels of *Tgf-β1* ($P < 0.01$), *Smad2* ($P < 0.05$), *Smad3* ($P < 0.01$), and *Sma* ($P < 0.05$) in the model and sham groups

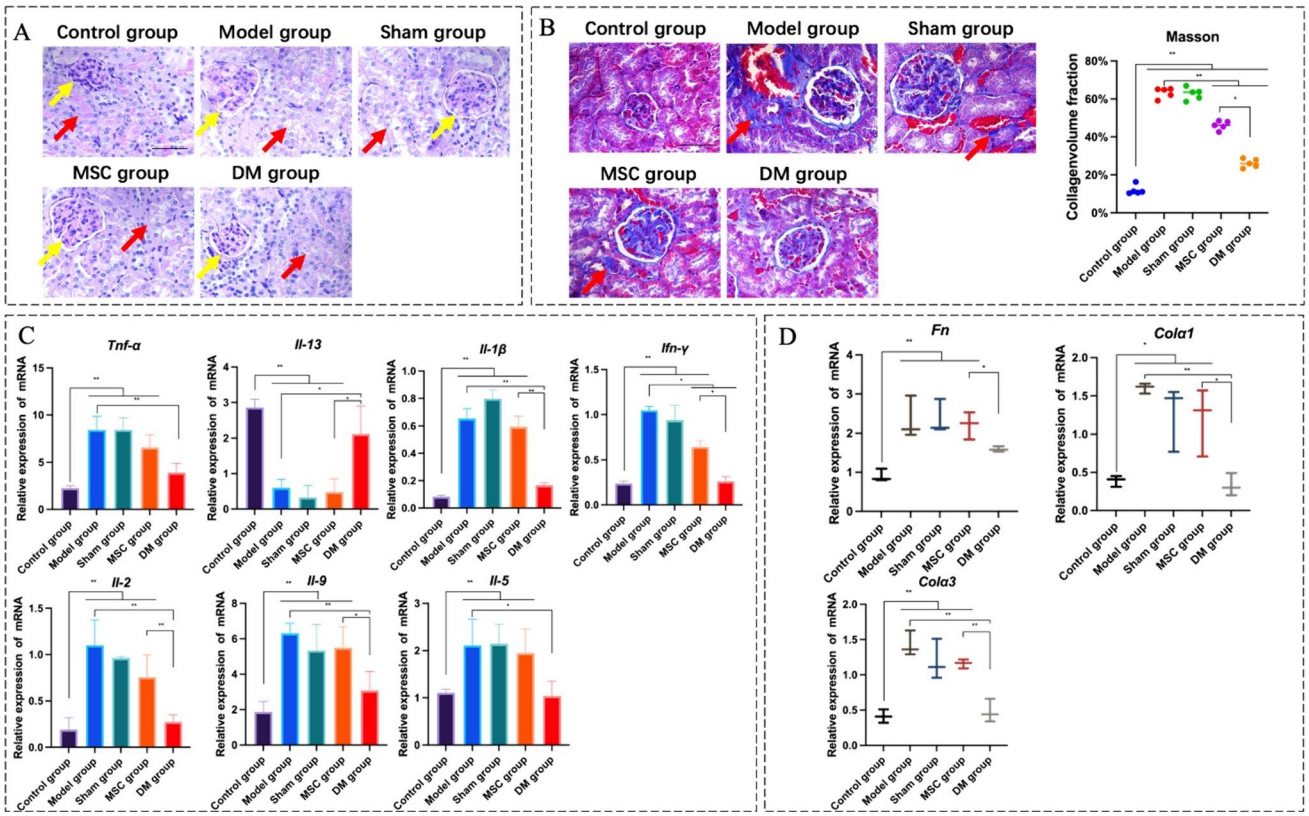

Fig. 6 Renal tissue histological examination and gene expression profiling. (**A**) Distribution of renal structure by PAS. The red arrows point to the position of glomeruli, and the yellow arrows to the brush border of renal tubules. (**B**) Level of renal fibrosis by Masson's trichrome. The red arrows point to the fibrosis. (**C**) Detection of gene expression of renal inflammatory factors (*Tnf-α*, *Il-13*, *Il-1β*, *Ifn-γ*, *Il-2*, *Il-9*, and *Il-5*) by qRT-PCR. (**D**) Detection of gene expression of renal fibrosis factors (*Fn, Colα1,* and *Colα3)* by qRT-PCR. Scale bar: 20 μm. Control group: C57BL/6 J mice. Model group: MRL/lpr mice. Sham group: MRL/lpr mice receiving saline treatment. MSC group: MRL/lpr mice receiving untreated hUC-MSCs. DM group: MRL/lpr mice receiving hUC-MSCs treated with 25 μmol/L DMOG. Except for the comparison with the MSC group by *t*-test, the rest of the data were analyzed by one-way ANOVA and expressed as mean ± SD ($n \geq 3$; *: $P < 0.05$, **: $P < 0.01$).

were increased (Fig. 7A). These factors are critical in the fibrotic process, indicating the activation of the TGF-β/Smad signaling pathway. The DM group exhibited more significant signs of mitigation than the MSC group. Compared to the model group, consistent protein distribution and expression patterns were observed, corroborating the mRNA expression findings ($P < 0.05$) (Fig. 7B–G). Elevated Tgf-β1, Smad2/3, p-Smad2, p-Smad3, and Sma protein expression further substantiated the activation of the TGF-β/Smad signaling pathway, which could be one of the driving factors behind renal tissue fibrosis in SLE model.

To validate whether DMOG-pretreated hUC-MSCs could promote repair by reducing fibrosis and inflammation, we conducted 3D co-culture experiments to delve deeper into the cellular functionality and molecular mechanisms, aiming to confirm the potential therapeutic effects of DMOG.

When observing the HEK 293 T cells morphology, we noted that following DMOG treatment, the HEK 293 T cells displayed a more aggregated and tightly connected appearance, with pronounced cell–cell adhesion when compared to the LPS group ($P < 0.05$) (Fig. 8A). These alterations in cellular morphology likely reflect the positive effects of DMOG on cell adhesion and interaction, crucial for its effectiveness in tissue repair. When examining these genes, it is essential to ensure the appropriateness of LPS treatment conditions. We chose a concentration of 10 μg/mL LPS for a 30-h treatment ($P < 0.05$) (Fig. 8B), a condition previously demonstrated to be optimal for inducing cellular inflammatory responses. Compared with the LPS group, *TNF-α* ($P < 0.01$) and *IL-6* ($P < 0.01$) were significantly decreased, and *IL-13* ($P < 0.05$) was significantly increased at the mRNA level in the DM group (Fig. 8C). We examined further the mRNA levels of factors associated with the TGF-β/Smad pathway in the DM group. We found them to be lower than in the LPS group, including *TGF-β1* ($P < 0.05$), *SMAD3* ($P < 0.01$), and *SMA* ($P < 0.01$) (Fig. 8D).

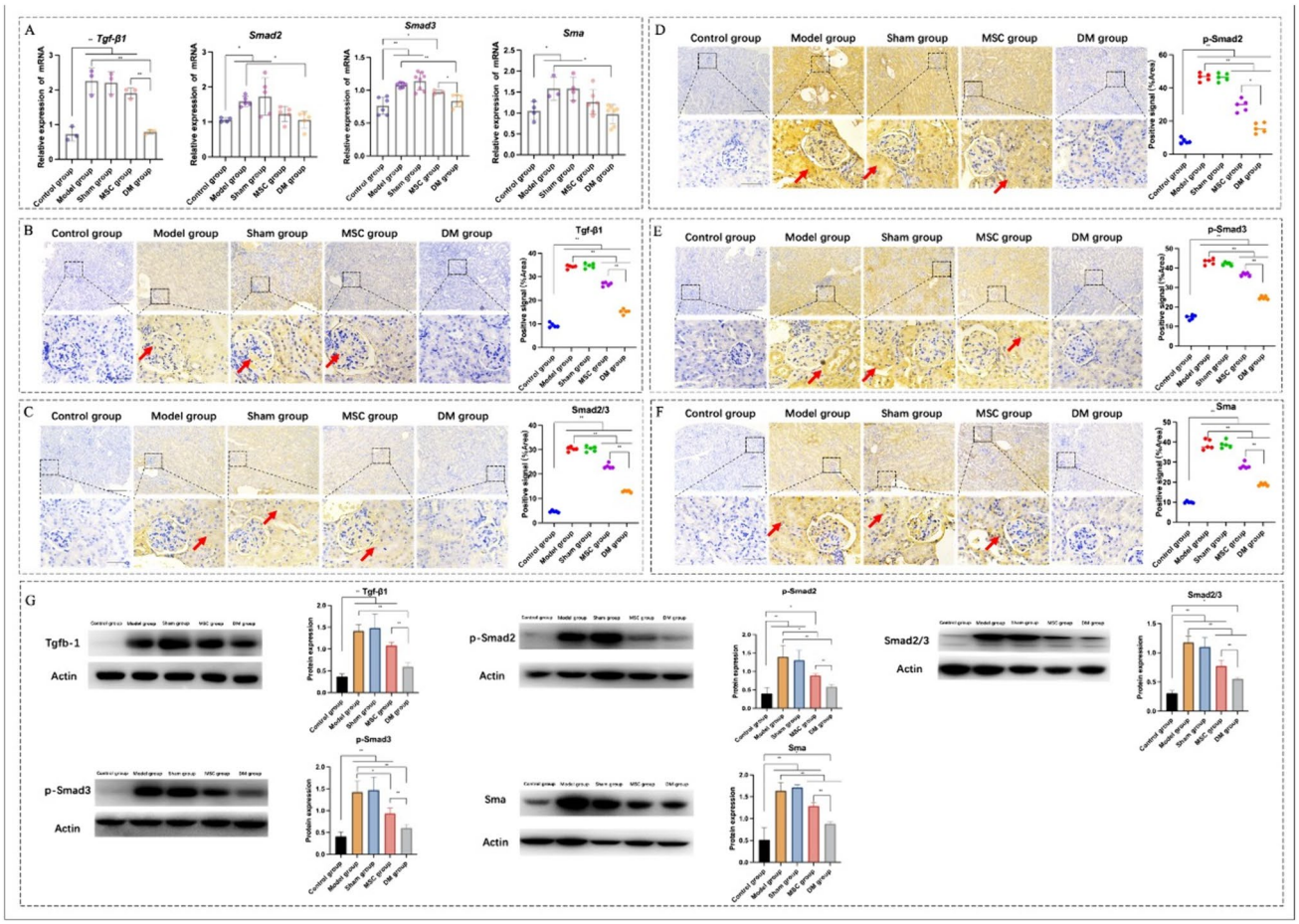

Fig. 7 Gene expression and protein profiling of TGF-β/Smad signaling pathway in renal tissue. (**A**) Detection of key gene expression (Tgf-β1, Smad2, Smad3, and Sma) of TGF-β/Smad in the kidney by qRT-PCR. (**B–F**) Immunohistochemistry detected the distribution of Tgf-β1, Smad2/3, p-Smad2, p-Smad3, and Sma in the kidneys. The red arrows point to positive signals. (**G**) Expression of key proteins (Tgf-β1, Smad2, Smad3, and Sma) of TGF-β/Smad) in the kidneys. Scale bar: 100 μm (top), 20 μm (bottom). Control group: C57BL/6 J mice. Model group: MRL/lpr mice. Sham group: MRL/lpr mice receiving saline treatment. MSC group: MRL/lpr mice receiving untreated hUC-MSCs. DM group: MRL/lpr mice receiving hUC-MSCs treated with 25 μmol/L DMOG. Except for the comparison with the MSC group by *t*-test, the rest of the data were analyzed by one-way ANOVA and expressed as mean ± SD ($n \geq 3$; *: $P < 0.05$, **: $P < 0.01$).

Discussion

Our initial experiments focused on characterizing the hUC-MSCs. The results confirmed their potential as multipotent hUC-MSCs based on their typical morphological features and expression of specific stem cell markers; they can differentiate into adipose and bone tissues. These findings are consistent with the definition of mesenchymal hUC-MSCs outlined in the 2023 International Society for Cell Therapy documentation [20] and solidify the groundwork for future investigations.

To investigate the effects of DMOG treatment on hUC-MSCs, it is essential to consider their role as immune sensors. This refers to the ability of MSC to suppress apoptosis when the immune system is overly active, preventing self-attack [21]. It has been reported that an LPS-induced in vitro cell model can mimic the inflammatory environment in LN [22–27]. This study used LPS to stimulate an inflammatory environment and analyze its impact on hUC-MSCs. Our results demonstrated that DMOG treatment effectively downregulated the expression of pro-inflammatory genes and upregulated the expression of anti-inflammatory genes. This regulatory effect suggests that DMOG treatment enhances the immunosensor functions of hUC-MSCs in response to immune challenges.

As mentioned earlier, inflammation plays a pivotal role in influencing the migratory behavior of hUC-MSCs. Based on this premise, our experiments yield noteworthy results. We observed that DMOG treatment had a significant positive effect on the migration and invasion of hUC-MSCs. The treated hUC-MSCs displayed an enhanced ability effectively to home to injured regions within the kidneys This outcome

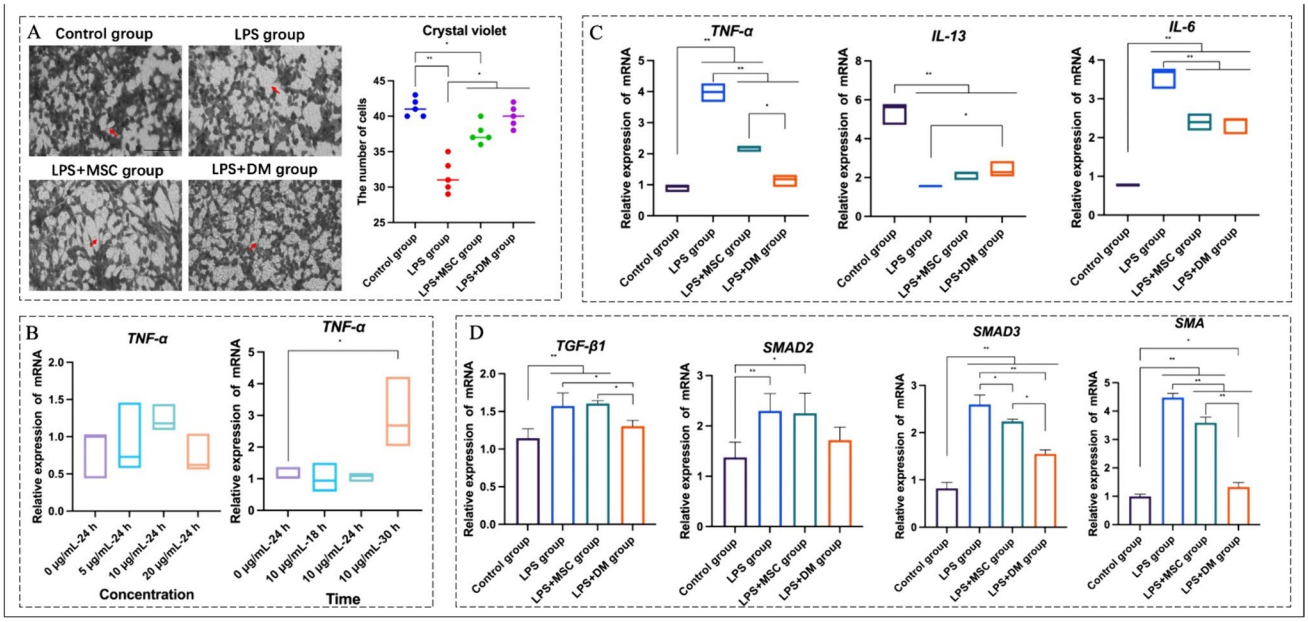

Fig. 8 Evaluating cellular morphology, fibrosis, and inflammation restoration following repair after 3D co-culture of HEK 293 T cells with DMOG-pretreated hUC-MSCs. (**A**) Status of HEK 293 T cells in 3D co-culture. Red arrows point to cells stained with crystal violet. Scale bar: 50 μm. (**B**) The concentration and time of LPS were measured in HEK 293 T cells by qRT-PCR for the *TNF-α* gene. (**C**) The gene expression of inflammatory factors (TNF-α, IL-13, and IL-6) was detected in HEK 293 T cells. (**D**) Detection of critical gene expression (*TGF-β1*, *SMAD2*, *SMAD3*, and *SMA*) of TGF-β/Smad in HEK 293 T cells. Control group: untreated HEK 293 T cells. LPS group: HEK 293 T cells treated with 10 μg/mL LPS. LPS + MSC group: Co-cultured HEK 293 T cells with hUC-MSCs treated with 10 μg/mL LPS. LPS + DMOG group: Co-cultured HEK 293 T cells with hUC-MSCs treated with 10 μg/mL LPS and 25 μmol/L DMOG. Except for the comparison with the MSC group by *t*-test, the rest of the data were analyzed by One-way ANOVA and expressed as mean ± SD ($n \geq 3$; *: $P < 0.05$, **: $P < 0.01$).

highlights the potential of DMOG to amplify their homing capabilities, which is of considerable significance in cell-based therapies.

In our disease model selection, we focused on SLE because of its relevance to stem cell therapies, that is, high-dose treatment supported by stem cell transplantation, which may lead to amelioration in experimental autoimmune disease models [28]. To maintain experimental comparability, we used MRL/lpr mice that exhibit lupus-like characteristics. Our initial study revealed promising results for DMOG-pretreated hUC-MSCs in inhibiting the enlargement of lymph nodes and restoring organ conditions, particularly in neck lymph nodes and kidney tissues, underscoring the potential of DMOG-pretreated hUC-MSCs in ameliorating organ abnormalities associated with SLE. We conducted histopathological examinations of the kidneys to gain deeper insights into these effects. HE staining, used to observe pathological changes in renal glomeruli, is a standard technique for evaluating the extent of tissue damage [29]. The results demonstrated a decrease in the infiltration of inflammatory cells within the renal glomeruli of hUC-MSCs treated with DMOG. Given the pivotal role of proteinuria [30] and immune biomarkers [31] in diagnosing, assessing, and managing SLE, urine and serum samples were collected to monitor urinary protein levels and hallmark SLE antibodies. The results revealed that a reduction in urinary protein content suggested a potential enhancement in kidney function and partial recovery of SLE hallmark antibody levels. Masson's trichrome staining was used to evaluate tissue fibrosis, and PAS staining to examine the restoration of glomerular basement membranes. Masson's trichrome staining indicated a reduction in kidney fibrosis, and PAS staining detected the restoration of glomerular basement membranes. Histopathological results obtained from renal biopsies are strongly associated with the clinical progression of LN [32], and damage to the lower class of renal biopsies signifies a milder disease state [33]. Differential gene expression levels of inflammatory cytokines and fibrotic markers can indicate renal restorative capacity [34]. A substantial recovery trend was evident in our analysis of the gene expression related to inflammation and fibrosis, with the most remarkable improvement observed in the DM group. This observation underscores the positive impact of the DMOG treatment on mitigating both inflammatory and fibrotic responses within the study's context.

As reported by Rachael et al., the fibrotic changes observed in LN are strongly associated with TGF-β1, suggesting a promising therapeutic target for addressing

LN-related fibrosis [35]. Extensive research has demonstrated that TGF-β1/Smad signaling pathway disruption is pivotal in kidney, liver, lung, and heart fibrosis pathogenesis. Smad-2 and Smad-3 have been identified as critical downstream modulators facilitating TGF-β1-mediated tissue fibrosis [36]. We explored the involvement of the TGF-β/Smad signaling pathway in renal fibrosis; results indicated activation of this pathway in the model and sham groups, whereas DMOG treatment mitigated its activation, suggesting a role in the renal protective effects of DMOG-pretreated hUC-MSCs. In the in vitro experiments, a 3D cell culture model of hUC-MSCs and kidney cells was established using transwell culture chambers, yielding conclusions consistent with those of the animal experiments. The in vitro experiments confirmed that DMOG treatment promoted cell adhesion and reduced inflammation and fibrosis. These findings further substantiate the potential of DMOG to enhance cellular functionality and regenerative capacity in stem cell-based therapies, thereby enhancing the credibility of this study.

This study employed a multifaceted approach involving animal models, in vitro cellular models, and investigations of molecular mechanisms to assess the effects of DMOG on hUC-MSCs; it aimed to provide more extensive datasets and deepen our understanding of the molecular mechanisms underlying these therapeutic effects. Such insights are valuable for guiding further research and clinical applications in stem cell therapy for SLE.

Acknowledgements We thank Editage (www.editage.cn) for editing the English language.

Authors' contributions All authors have materially participated in the research and/or article preparation and have approved the authenticity of the final article. MX and X HF conceived and designed the experiments. N AF, X NS, G CL, and D YC performed the experiments. N AF, Y XQ, WH, and G CY analyzed the data. N AF wrote the manuscript.

Funding This work was supported by the Research Fund of the National Research Institute for Family Planning (2023GJZD01) and Beijing Natural Science Foundation (No. 7222124).

Data Availability The datasets used or analyzed in the current study are available from the corresponding author upon reasonable request.

Declarations

Ethics approval and consent to participate The Institutional Animal Care and Laboratory Animal Welfare Ethics Committee of the National Research Institute for Family Planning approved all animal experiments and procedures.

Consent for publication Not applicable.

Competing interests The authors declare no competing interests.

References

1. Choi, M.Y., and K.H. Costenbader. 2022. Understanding the Concept of Pre-Clinical Autoimmunity: Prediction and Prevention of Systemic Lupus Erythematosus: Identifying Risk Factors and Developing Strategies Against Disease Development. *Frontiers in Immunology* 13: 890522. https://doi.org/10.3389/fimmu.2022.890522. (**Published 2022 Jun 3**).
2. Almaani, S., A. Meara, and B.H. Rovin. 2017. Update on Lupus Nephritis. *Clinical Journal of the American Society of Nephrology* 12 (5): 825–835. https://doi.org/10.2215/CJN.05780616.
3. Davidson, A. 2016. What is damaging the kidney in lupus nephritis? *Nature Reviews Rheumatology* 12 (3): 143–153. https://doi.org/10.1038/nrrheum.2015.159.
4. Bernatsky, S., J.F. Boivin, L. Joseph, et al. 2006. Mortality in systemic lupus erythematosus. *Arthritis and Rheumatism* 54 (8): 2550–2557. https://doi.org/10.1002/art.21955.
5. Weening, J.J., D'Agati, V.D., Schwartz, M.M., et al. The classification of glomerulonephritis in systemic lupus erythematosus revisited [published correction appears in J Am Soc Nephrol. 2004 Mar;15(3):835–6]. J Am Soc Nephrol. 2004;15(2):241–250. https://doi.org/10.1097/01.asn.0000108969.21691.5d
6. 3rd Austin, H.A., J.H. Klippel, J.E. Balow, et al. 1986. Therapy of lupus nephritis. Controlled trial of prednisone and cytotoxic drugs. *The New England Journal of Medicine* 314 (10): 614–619. https://doi.org/10.1056/NEJM198603063141004.
7. Yang, Q., Y. Liu, G. Chen, W. Zhang, S. Tang, and T. Zhou. 2021. An Overview of the Safety, Efficiency, and Signal Pathways of Stem Cell Therapy for Systemic Lupus Erythematosus. *Stem Cells International* 2021: 2168595. https://doi.org/10.1155/2021/2168595. (**Published 2021 Aug 13**).
8. Kaul, A., C. Gordon, M.K. Crow, et al. 2016. Systemic lupus erythematosus. *Nature Reviews Disease Primers* 2: 16039. https://doi.org/10.1038/nrdp.2016.39. (**Published 2016 Jun 16**).
9. De Becker, A., and I.V. Riet. 2016. Homing and migration of mesenchymal stromal cells: How to improve the efficacy of cell therapy? *World Journal of Stem Cells* 8 (3): 73–87. https://doi.org/10.4252/wjsc.v8.i3.73.
10. Shaughnessy, P.J., D.W. Ririe, D.L. Ornstein, et al. 2001. Graft failure in a patient with systemic lupus erythematosus (SLE) treated with high-dose immunosuppression and autologous stem cell rescue. *Bone Marrow Transplantation* 27 (2): 221–224. https://doi.org/10.1038/sj.bmt.1702767.
11. Chang, J.W., S.P. Hung, H.H. Wu, et al. 2011. Therapeutic effects of umbilical cord blood-derived mesenchymal stem cell transplantation in experimental lupus nephritis. *Cell Transplantation* 20 (2): 245–257. https://doi.org/10.3727/096368910X520056.
12. Lan, H.Y., and A.C. Chung. 2012. TGF-β/Smad signaling in kidney disease. *Seminars in Nephrology* 32 (3): 236–243. https://doi.org/10.1016/j.semnephrol.2012.04.002.
13. Wynn, T.A. 2008. Cellular and molecular mechanisms of fibrosis. *The Journal of Pathology* 214 (2): 199–210. https://doi.org/10.1002/path.2277.
14. Rosendahl, A.H., K. Schönborn, and T. Krieg. 2022. Pathophysiology of systemic sclerosis (scleroderma). *Kaohsiung Journal of Medical Sciences* 38 (3): 187–195. https://doi.org/10.1002/kjm2.12505.
15. Lan, H.Y. 2011. Diverse roles of TGF-β/Smads in renal fibrosis and inflammation. *International Journal of Biological Sciences* 7 (7): 1056–1067. https://doi.org/10.7150/ijbs.7.1056.
16. Zhou, B., T. Ge, L. Zhou, et al. 2020. Dimethyloxalyl Glycine Regulates the HIF-1 Signaling Pathway in Mesenchymal Stem Cells. *Stem Cell Reviews and Reports* 16 (4): 702–710. https://doi.org/10.1007/s12015-019-09947-7.

17. Chen, M.H., Y.H. Wang, B.J. Sun, et al. 2021. HIF-1α activator DMOG inhibits alveolar bone resorption in murine periodontitis by regulating macrophage polarization. *International Immunopharmacology* 99: 107901. https://doi.org/10.1016/j.intimp.2021.107901.
18. Sackstein, R. 2005. The lymphocyte homing receptors: Gatekeepers of the multistep paradigm. *Current Opinion in Hematology* 12 (6): 444–450. https://doi.org/10.1097/01.moh.0000177827.78280.79.
19. Zhang, L., C. Ye, P. Li, et al. 2022. ADSCs stimulated by VEGF-C alleviate intestinal inflammation via dual mechanisms of enhancing lymphatic drainage by a VEGF-C/VEGFR-3-dependent mechanism and inhibiting the NF-κB pathway by the secretome. *Stem Cell Research & Therapy* 13 (1): 448. https://doi.org/10.1186/s13287-022-03132-3. (**Published 2022 Sep 5**).
20. Viswanathan, S., K.L. Blanc, R. Ciccocioppo, et al. 2023. An International Society for Cell and Gene Therapy Mesenchymal Stromal Cells (MSC) Committee perspectives on International Standards Organization/Technical Committee 276 Biobanking Standards for bone marrow-MSCs and umbilical cord tissue-derived MSCs for research purposes. *Cytotherapy* 25 (8): 803–807. https://doi.org/10.1016/j.jcyt.2023.04.005.
21. Aggarwal, S., and M.F. Pittenger. 2005. Human mesenchymal stem cells modulate allogeneic immune cell responses. *Blood* 105 (4): 1815–1822. https://doi.org/10.1182/blood-2004-04-1559.
22. Chen, X.C., D. Wu, H.L. Wu, et al. 2022. Metformin improves renal injury of MRL/lpr lupus-prone mice via the AMPK/STAT3 pathway. *Lupus Sci Med.* 9 (1): e000611. https://doi.org/10.1136/lupus-2021-000611.
23. Li, D., G. Shi, J. Wang, et al. 2019. Baicalein ameliorates pristane-induced lupus nephritis via activating Nrf2/HO-1 in myeloid-derived suppressor cells. *Arthritis Research & Therapy* 21 (1): 105. https://doi.org/10.1186/s13075-019-1876-0. (**Published 2019 Apr 25**).
24. Tian, J., T. Huang, J. Chen, et al. 2023. SIRT1 slows the progression of lupus nephritis by regulating the NLRP3 inflammasome through ROS/TRPM2/Ca^{2+} channel. *Clinical and Experimental Medicine* 23 (7): 3465–3478. https://doi.org/10.1007/s10238-023-01093-2.
25. Liu, L., Y. Zhang, and L. Zhong. 2023. LncRNA TUG1 relieves renal mesangial cell injury by modulating the miR-153-3p/Bcl-2 axis in lupus nephritis. *Immunity, Inflammation and Disease* 11 (4): e811. https://doi.org/10.1002/iid3.811.
26. Xu, J.W., M.Y. Wang, Y. Mao, et al. 2024. Inhibition of STAT3 alleviates LPS-induced apoptosis and inflammation in renal tubular epithelial cells by transcriptionally down-regulating TASL. *European Journal of Medical Research* 29 (1): 34. https://doi.org/10.1186/s40001-023-01610-9. (**Published 2024 Jan 6**).
27. Xu, Z.Q., Y. Ding, X.Y. Huang, W. Xiang, and X.J. He. 2021. CircELK4 Contributes to Lupus Nephritis by Acting as a miR-27b-3p Sponge to Regulate STING/IRF3/IFN-I Signaling. *Inflammation* 44 (5): 2106–2119. https://doi.org/10.1007/s10753-021-01487-y.
28. Jantunen, E., and R. Myllykangas-Luosujärvi. 2000. Stem cell transplantation for treatment of severe autoimmune diseases: Current status and future perspectives. *Bone Marrow Transplantation* 25 (4): 351–356. https://doi.org/10.1038/sj.bmt.1702152.
29. Yu, C., P. Li, X. Dang, X. Zhang, Y. Mao, and X. Chen. 2022. Lupus nephritis: New progress in diagnosis and treatment. *Journal of Autoimmunity* 132: 102871. https://doi.org/10.1016/j.jaut.2022.102871.
30. Gasparotto, M., M. Gatto, V. Binda, A. Doria, and G. Moroni. 2020. Lupus nephritis: Clinical presentations and outcomes in the 21st century. *Rheumatology (Oxford)* 59 (Suppl5): v39–v51. https://doi.org/10.1093/rheumatology/keaa381.
31. Yu, H., Y. Nagafuchi, and K. Fujio. 2021. Clinical and Immunological Biomarkers for Systemic Lupus Erythematosus. *Biomolecules.* 11 (7): 928. https://doi.org/10.3390/biom11070928. (**Published 2021 Jun 22**).
32. Moroni, G., P.G. Vercelloni, S. Quaglini, et al. 2018. Changing patterns in clinical-histological presentation and renal outcome over the last five decades in a cohort of 499 patients with lupus nephritis. *Annals of the Rheumatic Diseases* 77 (9): 1318–1325. https://doi.org/10.1136/annrheumdis-2017-212732.
33. Bajema, I.M., S. Wilhelmus, C.E. Alpers, et al. 2018. Revision of the International Society of Nephrology/Renal Pathology Society classification for lupus nephritis: Clarification of definitions, and modified National Institutes of Health activity and chronicity indices. *Kidney International* 93 (4): 789–796. https://doi.org/10.1016/j.kint.2017.11.023.
34. Yung, S., and T.M. Chan. 2017. Anti-dsDNA antibodies and resident renal cells - Their putative roles in pathogenesis of renal lesions in lupus nephritis. *Clinical Immunology* 185: 40–50. https://doi.org/10.1016/j.clim.2016.09.002.
35. Wright, R.D., P. Dimou, S.J. Northey, and M.W. Beresford. 2019. Mesangial cells are key contributors to the fibrotic damage seen in the lupus nephritis glomerulus. *Journal of Inflammation (London)* 16: 22. https://doi.org/10.1186/s12950-019-0227-x. (**Published 2019 Nov 14**).
36. Hu, H.H., D.Q. Chen, Y.N. Wang, et al. 2018. New insights into TGF-β/Smad signaling in tissue fibrosis. *Chemico-Biological Interactions* 292: 76–83. https://doi.org/10.1016/j.cbi.2018.07.008.